Journal of Materials Chemistry C

Band-edge modulated ZnO Pomegranates-on-Paper Photodetector

Journal:	*Journal of Materials Chemistry C*
Manuscript ID:	TC-ART-12-2014-002787.R1
Article Type:	Paper
Date Submitted by the Author:	08-Feb-2015
Complete List of Authors:	Li, Haili; Harbin Institude of Technology, Jiao, Shujie; Harbin Institute of Technology, Li, Hongtao; Harbin Institude of Technology, Li, L.; Harbin Normal University, Key Laboratory of Photonic and electronic Bandgap materials, Ministry of Education Zhang, Xitian; Harbin Normal University, Key Laboratory of Photonic and electronic Bandgap materials, Ministry of Education; The Chinese University of Hong Kong, Department of Physics

Journal of
Materials Chemistry C

Cite this: DOI: 10.1039/c0xx00000x

ARTICLE TYPE

www.rsc.org/xxxxxx

Band-edge modulated ZnO Pomegranates-on-Paper Photodetector

Haili Li[a], Shujie Jiao*[a,b], Hongtao Li[a], Lin Li[b] and Xitian Zhang[b]

Received (in XXX, XXX) Xth XXXXXXXXX 20XX, Accepted Xth XXXXXXXXX 20XX
DOI: 10.1039/b000000x

Abstract: Recently, significant progresses have been achieved in paper electronics due to their potential technological applications in rollup displays, wearable devices and smart cards. However, it is still a challenge to form suitable structured materials on paper substrates efficiently due to their porous and rough surface. In this research, ZnO pomegranates composed by 8 nm ZnO nanodots have been fabricated on pencil drawn graphite-on-paper substrate successively by an eco-friendly and cost effective solvothermal method. Most significantly, this solution grown photoconductive photodetector shows good device performances with spectrum responsivity to ultraviolet light 0.06 A W^{-1} and quick response time 4.3 s. Systematic analysis shows that the interface-related energy boundary modulation within ZnO pomegranates may facilitate the separation of photo-induced carriers, eventually results in its low dark current and quick response. Meanwhile, this structure designing strategy can be utilized for future fabrication of high performance paper electronics with other materials. Besides, due to firm attachment of ZnO pomegranates on substrate caused by the introduction of ethanol during solvothermal growth process and ultrasonic vibration during the formation of ZnO seed layer, this device is also a largely flexible and rolled-up photodetector with good reversible characteristic and steady performance to bending deformations and irradiation degration.

KEYWORDS: Flexible Photodetector, Paper electronic, ZnO nanostructure, Band-edge modulation

Introduction

Ever-increasing modern consumer electronics demand an improvement in multi-functionality and flexibility. Flexible and portable electronics, which interface well with human beings, have been the emerging research focus in recent years such as wearable device, electronic paper, chip smart cards and basic components in various devices.[1-5] But fabrications of optoelectronic devices on flexible substrates are just beginning to emerge from research laboratories and have not yet to be commercialized widely.[6-10] Suitable substrates, which are indispensable for fabrications of flexible devices, are essential for their cost-effective and eco-friendly applications. Paper substrate is a good candidate in terms of its superior advantages including environmentally benign, renewable, light weight, three-dimensional fibrous structure, available all over the world and inexpensive price as well. In recent years, paper electronic has attracted enormous attention,[11] especially for quick response and high sensitivity paper-based photodetectors, which combine the portable and flexible properties of paper substrate and the wide applications of photodetector in military and civilian areas. But only a few reports are available. The main challenge is the feasible and efficient fabrications of light absorption materials and electrodes on the porous and thin paper substrate owing to its rough surface and flammability, which eventually results in poor performance of paper electronic devices. Analyzing from this point, suitable structure designing of materials, which can coincide well with rough substrate, are of great significance. It is believed that layered graphite, which are high conductivity and can be steadily attached onto paper substrate, would be good candidate for electrode materials. The graphite-on-paper (G-P) substrate used in this report is formed by drawing interdigital graphite electrodes directly on paper. As for light absorption materials, ZnO is a good candidate in terms of its versatile morphologies and diverse processing technologies besides its inherent nature of wide band gap (3.37 eV), large exciton binding energy and resistance to radiations.[12,13] While in order to match the performance of conventional devices, ZnO nanomaterials with suitable size and structure, which should be ideally compatible with paper while maintaining low cost, flexibility and high performance, are urgently needed. Considering the fibrous and porous structure of paper, sphere-like ZnO nanomaterials would be an excellent choice. To be more specific, pomegranate-like ZnO is highly desired based on the rational that grains or grain boundaries may serve as energy barriers and facilitate the separation of electrons and holes by introducing additional band-edge modulation.[14]. Indeed, the formation of silicon pomegranates has been reported in Nat. Nanotech. by Nian Liu, et. al, in 2014,[15] while reports on ZnO pomegranate-based devices are rarely few.

In this report, ZnO pomegranates are fabricated on G-P substrate

through a "green" and cost effective solvothermal method with ethanol as solvent. Besides the formation of desired ZnO pomegranates, the mechanical property of the hygroscopic paper substrate was well maintained by using ethanol as solvent instead of water. At the same time, the high pressure caused by the lower boiling point ethanol solvent during the crystal growth process also strengthened the adhesion between ZnO pomegranates and G-P substrate. To further improve the adhesion and distribution of ZnO on G-P substrate, ultrasonic vibration was introduced during the formation of ZnO seed layer. Detail procedures for fabrication of G-P based ZnO ultraviolet (UV) detector are illustrated in Fig. 1. Systematic explorations show that the as-synthesized device has not only low dark current, visible-blind and reproductivity characteristics, but also good sensitivity and short response time.

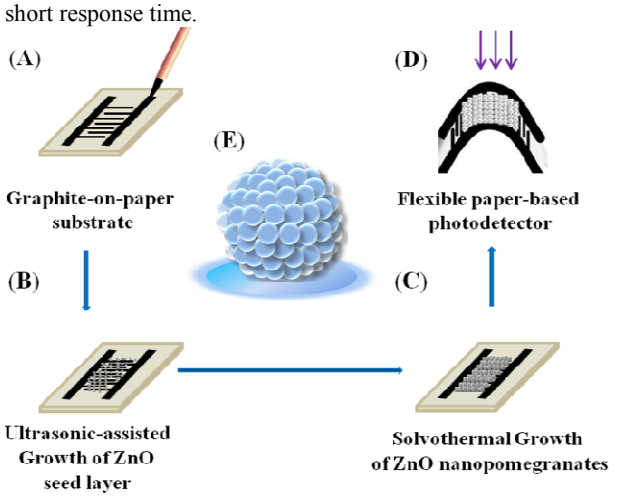

Fig. 1 Schematic graph for fabrication of G-P based ZnO UV detector. A) Formation of G-P substrate by drawing graphite traces on paper. B) Ultrasonic-assisted growth of ZnO seed layer. C) Solvothermal growth of ZnO pomegranates on the as-synthesized substrate. D) Schematic diagram of the as-synthesized flexible photodetector. E) Schematic diagram of the as-synthesized ZnO pomegranate composed of small size ZnO nanodots.

Experimental Section

Fabrication of G-P based ZnO UV detector: A piece of common used writing paper with thickness 0.1 mm was used. Graphite interdigital electrodes were drawn on paper using 9B pencil (Raffine, schetch 7001). The sol-gel solution for ultrasonic-assisted growth of ZnO seed layer was prepared as mentioned before.[16] The G-P substrate was sunk into the sol-gel for 30 min before being treated in ultrasonic instrument (Kunshan, KQ-50B, 40 KHz) for 20 min and dried at 150 ^{o}C for 30 min eventually. ZnO seed layer was formed by repeating these procedures for three times and ZnO pomegranates were formed on the substrate by solvothermal method at 90 ^{o}C for 12 h with ethanol as solvent. The nutrient solution was consisted of zinc acetate dihydrate ($Zn(CH_3COO)_2 \cdot 2H_2O$, 0.025 M) and hexamine (HMT, 0.025 M). After being thoroughly rinsed by pure ethanol, the device was dried in the air for 30 min and then heated in the electric thermostatic drying oven at 150 ^{o}C for 30 min.

Characterizations: Scanning electron microscope (SEM, KYKY-EM6000C, 15 KV) and Transmission electron microscope (TEM, Hitachi, H-7650) were used for structure characterization. The composition and crystalline analyses were achieved by Bruker's Energy Disperse Spectroscopy (15 kV), HORIBA Jobin Yvon' Raman spectrometer (LabRAM HR800, excited wavelength 488 nm) and X'Pert Pro MPD X-ray diffractometer (Philips-FEI, Netherlands, Cu Ka radiation). The spectral response test of the as-synthesized UV detector was performed by Zolix's solar cell quantum efficiency testing system (SolarCellScan 100). I-V and time response spectrum of the as-synthesized device was measured by the electrochemical workstation (Corrtest, CS350) with a three electrodes system. The device's flexitivity and reproductivity were measured by attaching device to a flexible plastic template and folding the template to different bending angles.

Results and Discussion

SEM image of the G-P substrate is illustrated in Fig. 2A and the pencil-drawn interdigital electrode composed of two graphite electrodes (2 mm wide and 3 mm long) and a 0.5 mm-wide spacing gap between them (paper spacing) is exhibited. The intrinsically rough and porous surface of paper, which is considered as one of the obstructions for development of paper electronics, is exhibited in high magnification SEM micrograph of paper section in Fig. 2B. Fig. 2C is the high magnification SEM micrograph of graphite electrodes, which confirms the possibility of fabricating optoelectronic devices on this G-P substrate by showing a well distributed graphite traces on paper substrate. With solvothermal method, ZnO are formed on the whole G-P substrate as shown in Fig. 2C. In paper spacing (Fig. 2E), ZnO nanomaterials form both on cellulose fibers and within the fibrous holes. The distribution of ZnO spheres on paper fibers is given by higher magnification SEM in the inset of Fig. 2E. As for graphite electrodes, thick ZnO films are formed as shown in Fig. 2F.

Detail analysis on the structure of ZnO was performed by TEM characterization. As shown in Fig. 3A and Fig. 3B, ZnO nanospheres with average diameter 400 nm are observed. Fine structure of these ZnO nanospheres is analyzed by high magnification TEM in Fig. 3C, which confirms the formation of ZnO pomegranates by exhibiting a ZnO sphere consisted of ZnO nanodots with average diameter 8 nm. Selected area electron diffraction (SEAD) pattern of ZnO pomegranate shown in Fig. 3D indicates its polycrystalline structure**.** Fig. 3E is HRTEM image of one of nanodots. The highly ordered lattice confirms the formation of highly crystalline ZnO nanodots.

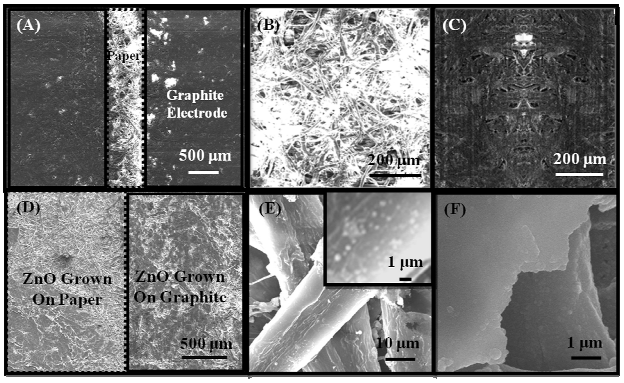

Fig. 2 A) SEM image of G-P substrate. B) and C) High magnification SEM images of paper spacing and graphite electrode. D) SEM image of ZnO nanomaterials grown on the G-P substrate. E) and F) High magnification SEM images of ZnO nanomaterials formed on paper section and graphite electrode, respectively. The inset of Fig. 2E) shows the higher magnification SEM of ZnO nanospheres on paper fibers.

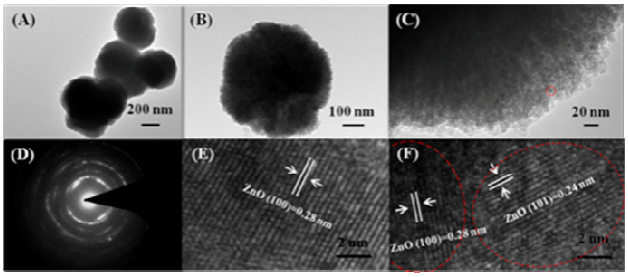

Fig. 3 A)-C) TEM micrographs of ZnO pomegranates. The red circle in C) marks one of ZnO nanodots. D) SEAD image of the edge section of ZnO pomegranate. E) and F) HRTEM images of ZnO nanodots within ZnO pomegranates. HRTEM images marked by red circles in F) belong to two separated ZnO nanodots.

HRTEM image in Fig. 3F is taken from the interface boundaries of ZnO nanodots and multiple sets of diffraction fringes are observed. The lattice spacing marked by red curves in Fig. 3F are measured to be 0.24 nm and 0.28 nm, which belong to (101) and (100) planes of wurtzite ZnO.[17-18]

In the X-ray diffraction spectrum (XRD) of the as-synthesized device (Fig. 4A), high intensity diffraction peaks at 31.78°, 34.42° and 36.24°, which can be well indexed to wurtzite ZnO (JCPDS No. 36-1451).[19,20] are observed besides the weak peaks from graphite (JCPDS No. 26-1079) and $CaCO_3$ in paper (JCPDS No. 47-1743). The appearance of multipeaks of ZnO accords well with the polycrystalline structure of ZnO pomegranates.[21] Besides, Scherer formula is also introduced for estimation of the average grain size of ZnO nanodots as shown in Equation 1: [22]

$$D = \frac{0.89\lambda}{B\cos\theta} \quad (1)$$

where D, λ, θ and B are the mean grain size, the X-ray wavelength of 0.154 nm, the Bragg diffraction angle and the full width at half maximum (FWHM) of (1 0 0), (0 0 2) and (1 0 1) peaks, respectively. The average grain size is calculated to be 10 nm, which is in good accordance with TEM results.

Detail information on the material quality and purity is illustrated by Raman spectrum shown in Fig. 4B. In its Raman spectrum, typical Raman diffraction peaks of ZnO are obtained accompanied by weak peaks from paper and graphite.[23-25] Generally, wurtzite ZnO belongs to the C_6v ($P6_3mc$) space group and has 12 degrees of freedom including 9 optical phonon modes and 3 acoustic phonon modes. Group theory predicts that the optical phonon modes at the point of the Brillouin zone (BZ) belong to the following irreducible representation: $\Gamma_{opt} = 1A_1 + 2B_1 + 1E_1 + 2E_2$ and the frequencies of the fundamental optical modes in ZnO includes: E_2 (low) = 101 cm^{-1}, E_2 (high) = 437 cm^{-1}, A_1 (TO) = 380 cm^{-1}, A_1 (LO) = 574 cm^{-1}, E_1 (TO) = 407 cm^{-1}, and E_1 (LO) = 581 cm^{-1}.[25] Herein, E_2 (high)
optical mode is observed. Meanwhile, peak from E_1 (LO) mode, which is closely associated with defects, is also obtained.[26,27] The relatively weaker peak at 581 nm illustrates that low concentration defects exist. This can be further confirmed by the

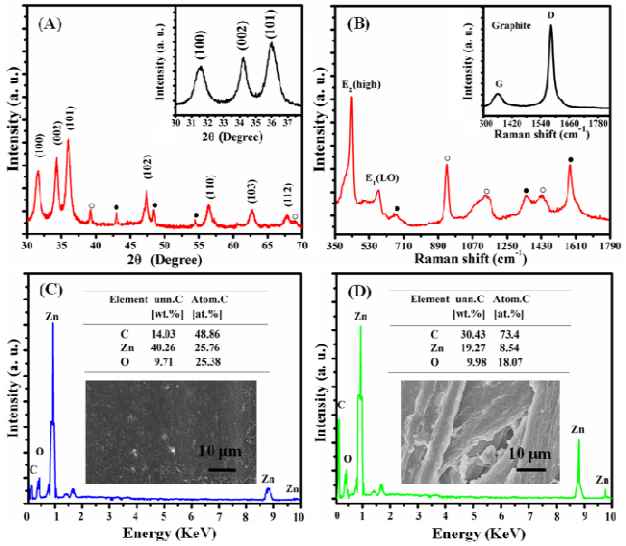

Fig. 4 A) and B) XRD and Raman spectra of the as-synthesized ZnO nanomaterials on G-P substrate. The peaks marked by hollow and solid circles belong to paper and graphite, respectively. Inset curves in A) and B) are the selected XRD peaks for ZnO and raman peaks for G-P substrate. C) and D) EDS spectra of ZnO formed on the graphite electrodes and paper spacing. The inset micrographs show images of the selected sections in EDS tests. The inset tables show the corresponding mass ratio and atom ratio of Zn/O atoms.

Energy Disperse Spectroscopy (EDS) in Fig. 4C-4D. To some extent, the nonstoichiometric Zn/O atom ratio for ZnO nanomaterials formed on the paper substrate could explain the formation of defects. Together with the patterned HRTEM of ZnO nanodots, it is rational to deduce that defects mainly exist on the surface of nanodots or within their grain boundaries.

Fig. 5A is the spectral response spectrum of G-P substrate and the as-synthesized ZnO pomegranates photodetector on it. It is obvious that G-P substrate shows no responsivity to light illumination by exhibiting a continued low values to wavelength variations from 300 nm to 550 nm. In comparison, with ZnO pomegranates formed on the G-P substrate as light absorption materials, the as-synthesized device shows a high degree of visible blindness with UV (354 nm) to visible (460 nm) rejection ratio 25. For wavelength shorter than 354 nm, the device shows a relatively high responsivity, then the responsivity drops down and reaches its lowest values at wavelength of 400 nm. The device's visible-blindness characteristic is exhibited by maintaining a low responsivity to wavelength ranging from 400 nm to 550 nm. Besides, its responsivity also increases significantly with bias voltage as shown in the inset spectrum of Fig. 5A. Fig. 5B is the time response spectrum of this paper-based device to UV light. In this spectrum, the device responds quickly to UV light exposure at first and then slowly reaches saturation value. When the UV light is turned off, the photocurrent decays in a relatively slower rate. According to the definition of photoresponse time, the time for photoresponse rised by 63% and dropped by 37% from the maximum current is 4.3 s and 14 s, which is about 1000 times quicker than paper-based ZnO nanorods photodetector.[11] Generally, there are mainly three speed limitations for

photodetectors fabricated on defect-free materials: transit time across the depletion region, RC time constant and diffusion of photogenerated carriers in low-field regions. Photoconductive detector does not suffer from RC time constant and diffusion of photogenerated carriers in low-field regions. Thus, transit time ($T_{(TR)}$) may be the limitation and can be estimated by Equation 2:[28]

$$T_{(TR)} = L^2 / V\mu_n \quad (2)$$

Where L is the contact separation, V is applied bias and μ_n is the electron mobility (estimated 1 $cm^2\ V^{-1}\ s^{-1}$).[29] The calculated $T_{(TR)}$ under bias of 9 V is around 300 μs, which partly contributes to the time constants. Thus, there must be other reasons dominate this response process. This deduction can be proved by the second order exponential decay fitting function shown in Equation 3.[30]

$$I_{(ph)}(t) = I_{(ph)}(\infty) + A_1 e^{-t/\tau_{d1}} + A_2 e^{-t/\tau_{d2}} \quad (3)$$

where A_1, A_2 are positive constants and $I_{(ph)}(\infty)$ refers to the photocurrent after infinitely long decay time, which essentially is the dark current. The τ_{d1} and τ_{d2} are time constants. The calculated $I_{(ph)}(\infty)$ and time constants τ_{d1} and τ_{d2} are 3.4 μA, 6.7 s and 22.4 s, which are in the same magnitude of the experimental result. Due to the large surface to volume ratio of ZnO nanomaterials, trapping at surface states, which mainly refers to the oxygen adsorption and desorption process at the surface of ZnO pomegranates, may play a key role in the its response process as illustrated in Fig. 5C.

Compared to the relatively longer response time of nanorod-based photoconductive photodetector,[11] further explorations on the working mechanism of this pomegranates-based photodetector is necessary. The electrical property of the as-synthesized device is shown in Fig. 5D. As exhibited by the black curve, a low dark current at the magnitude of nA is obtained for the as-synthesized paper-based device. While a higher photocurrent is obtained when the device is illuminated under UV light, which guarantees its good responsivity to UV illumination. In comparison, G-P substrate shows no response to UV light as its photocurrent and dark current are nearly with the same values. Its photocurrent measured under UV illumination is given by the purple curve in Fig. 5D, which coincides with the dark current curve of ZnO pomegranate-based photodetector. It should be noted that both schottky and ohmic contact between ZnO and graphite are already obtained in previous researches. The specific contact type is in close relationship with the face-dependent work functions of ZnO (4.25, 4.64, and 4.95 eV) and the work functions of graphene (4.32–5.08 eV) depending on the layer number and doping.[31] Herein, the linear I-V curve of the device under UV illumination indicates the formation of photoconductive UV detector and confirms the key role of oxygen absorption and desorption process (at the surface of ZnO pomegranates) in the photo response process of the as-synthesized devices.[31] Thus, the reduced response time of ZnO pomegranates-on-paper photodetector is believed to be mainly caused by the introduction of pomegranate-like structure of ZnO. The crystalline grains and grain boundaries between each ZnO nanodot, which lead to the formation of energy barriers for carrier transport within ZnO pomegranates and increase the resistance of

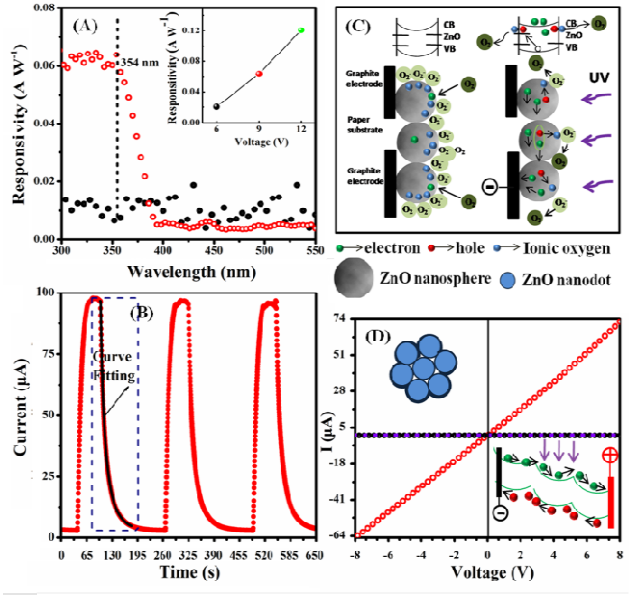

Fig. 5 A) Spectral response of the G-P based ZnO UV detector with optical power 150 mW cm^{-2} at 9 V bias voltage, the inset picture shows the voltage dependence of responsivity. B) Temporal photocurrent response to UV light ON-OFF cycles (red curve) and the selected-section curve fitting (black curve) at 9 V bias voltage. C) Schematic graph of oxygen adsorption and desorption process at the surface of ZnO pomegranates. D) I-V curves measured in the dark (black curve) and with UV illumination (red curve). The inset images are the schematic diagrams of cutway picture of the inside of the as-synthesized ZnO pomegranates and the grain boundary-related band-edge modulation caused by grains and grain boundaries within ZnO pomegranates. The UV light used in Fig. 5B and Fig. 5D is 365 nm with light power 20 mW cm^{-2}.

the photodetector in dark environment. Besides, as illustrated by X. Liu in Nat. Comm.,[15] these grain boundaries also introduce additional band-edge modulation within the ZnO pomegranates, which prompts separation of photocarrierss and facilitate the collection of photocurrent as shown in inset diagrams in Fig. 5D. Consequently, when UV light is turned on, a much higher photocurrent is obtained.

Based on the above analysis, working mechanism of the as-synthesized device can be illustrated as follows: In dark condition, oxygen molecules from the air are easily stuck on the surface of ZnO pomegranates by adsorption process and trap electrons available on the surface [$O_2\,(g) + 2e^- \rightarrow O^{2-}$]. Formation of large number of ionized oxygen leads to the formation of depletion layer in superficial ZnO nanodots and consequently results in the band bending of conduction band and valence band. Generally, the O_2 related depletion layer on the ZnO surface is estimated to be 1-3 nm,[32] which means that the depletion region is sufficient for the 8 nm ZnO nanodots on the surface of ZnO pomegranates. Together with the grain boundary-related energy barriers within the ZnO pomegranates,[14] the resistance of the device is largely increased, which well explains the low dark current at the magnitude of nA.[30] When the device is exposed to UV illumination, electron-hole pairs are generated by light absorption [$h\nu \rightarrow e^- + h^+$]. Holes migrate to the surface along the potential

gradient produced by band-bending to combine with the ionic oxygen ($O^{2-} + 2h^+ \rightarrow O_2$ (*g*)) and release oxygen molecules. The electrons generated in this process contribute to the increase in its photoconductivity. The boundary-related band-edge modulation within ZnO pomegranates contributes to the separation of photoelectrons and holes and the transformation of carriers as well. As a consequence, a high sensitivity UV detector is achieved. It is noteworthy that there are still excess holes left and recombine with free electrons resulting in the presence of the obtuse shape in the rise time. Together with the re-adsorption of few of the released oxygen molecules, a statured photocurrent value is achieved after a certain time when the electron-hole generation rate and oxygen re-adsorption rate become constant. Here, the high photocurrent is mainly maintained by nanodots, which prompt the separation of electrons and holes and suppress carriers recombination processes.[14] During photocurrent decay, the exciton related electron-hole recombination dominates the faster decay component. But there are still unpaired electrons left in ZnO. Oxygen molecules are gradually captured by these electrons and reabsorbed on the surface resulting in the slow decay process.[33] Besides, it is well-believed that adsorption process of oxygen is slower than its photodesorption process, which well explains the longer decay time compared with the rising time.[30] To further improve the device performance of this paper electronic device, the effect of the width of graphite electrode on the performance of paper-based photodetector was also studied in Supporting Information, which proves that the device performance can also be influenced by electrode parameters. Thus, it is believed that an excellent G-P based ZnO UV detector can be achieved by further combining ink-printed method to produce nano-scale graphite electrodes.[34]

The great potential of ZnO pomegranate-like structure for high-performance UV detection is explored by the above investigations. This structure can also be used to design high-performance photodetectors with other material systems. Meanwhile, the device's flexibility and toughness are equally important for flexile devices and worth researching. Fig. 6A is I-V curve measured at different bending angles and the inset of Fig. 6A shows the schematic diagram of bending device. Fig. 6B shows the bending angles-dependent variations of photocurrent with respect to the non-bending I-V curve measured at different bias voltages. All thses two spectra confirm the good robustness of the as-synthesized device to bending deformations. The device's reversible ability is exhibited in Fig. 6C, which exhibits steady performance with only slight decrease in photocurrent even after being bended for 150 times. What's more, the stability of this photodetector to long time UV irradiation (365 nm) is also tested in Fig. 6D, which shows slight irradiation degradation within 9 h and only 40% drop off in photocurrent is obtain after 12 h ultraviolet illumination. All these results indicates that ZnO pomegranates and this chemical bath deposition method can be potentially used for low-cost flexible and portable devices in future.

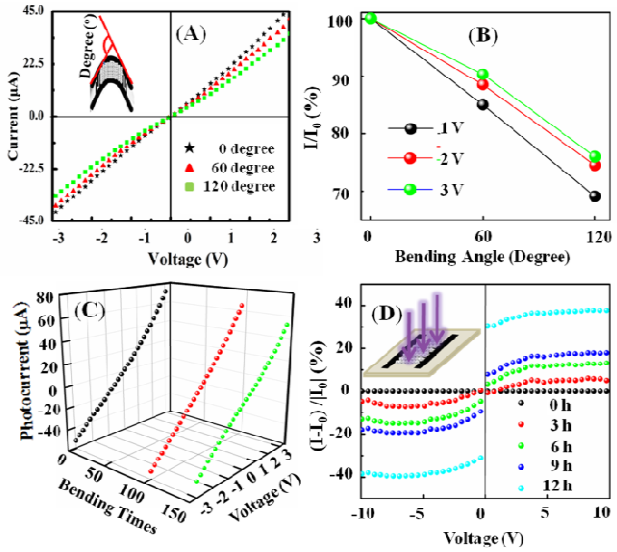

Fig. 6 A) I-V curve of the device measured at different bending angles. The inset of Fig. 6A is the schematic diagram of the bending device. B) Bending angles -dependent photocurrent variations measured at different bias voltage. C) I-V curves of the device measured after being bended for different times. D) Stability characterization of paper-based photodetector to ultraviolet irradiation.

Conclusion

In conclusion, high performance photoconductive UV detector has been fabricated on G-P substrate by green solvothermal method. With pencil-drawn graphite electrodes on paper as electrodes and ZnO pomegranates as light adsorption material, this device shows good sensitivity, quick response and visible blind characteristics. All these good properties also pave a way for fabrications of high performance paper-based electronics by tuning the structure and size of related materials. Herein, the boundary induced energy-edge modulation of ZnO pomegranates is highlighted. Most significantly, the device exhibits steady performance at different bending curvatures, good reproducibility property and resistance to UV radiation. All these excellent performances, as well as the systematically fundamental analysis on the mechanism of this paper-based ZnO photodetector, promise a way for fabrications and applications of high performance paper based electronic devices.

Funding Sources

This work is supported by National Science Foundtion (No. 61306014); Harbin Special Fund for Creative Talents in Science and Technology (No. 2012RFLXG029); Research Fund for the Doctoral Program of Higher Education of China (No. 20122302120009); Open Project Program of Key Laboratory for Photonic and Electric Bandgap Materials, Ministry of Education, Harbin Normal University, (No. PEBM201302).

Notes and references

[a] School of Materials Science and Engineering, Harbin Institute of Technology, Harbin 150001, P. R. China;
[b] Key Laboratory for Photonic and Electric Bandgap Materials, Ministry of Education, Harbin Normal University, Harbin 150025, P. R. China.
* Corresponding author: E-mail: shujiejiao@gmail.com

Electronic Supplementary Information (ESI) available: [Graphite-on-paper based ZnO ultraviolet detector formed by hydrothermal method. The effects of the structure of ZnO, ultrasonic vibration for the formation of ZnO seed layer and the width of graphite electrode on device's performance were also studies]. See DOI: 10.1039/b000000x/

1 J. G. Mccall, T-K. G. Shin, X. Huang, Y. H. Jung, R. Al-Hasani, F. G. Omenelto, M. R. Bruchas and J. A. Rogers, *Nature,* 2013, ***8***, 2413-2428; S. H. Wang, L. Lin and Z. L. Wang, *Nano Lett.*, 2012, ***12***, 6339.

2 I-W. P. Chen, S-H. S. Jhou, S. Jhou and Y-W. Chen, *J. Mater. Chem. C*, 2013, **1**, 5970-5975; H. Koga, M. Nogi, N. Komoda, T. T. Nge, T. Sugagara and K. Suganuma, *NPG. Asia. Mater.* ,2014, ***6***, e93.

3 H. Jin, J. Zhou, X. L. He, W. B. Wang, H. W. Guo, S. R. Dong, D. M. Wang, Y. Xu, J. F. Geng, J. K. Luo and W. I. Miline, *Nature,* 2013, ***3***, 2140; S. Wünscher, R. Abbel, J. Perelaer and U. S. Schubert , *J. Mater. Chem. C*, 2014, ***2***, 10232.

4 L. Zhang, J. W. Deng, L. F. Liu, W. P. Si, S. Oswald, L. X. Xi, M. Kundu, G. Z. Ma, T. Gemming, S. Baunack, F. Ding, C. L. Yan and O. G. Schmidt, *Adv. Mater.,* 2014, ***26***, 4527.

5 L. Li, H. Lu, Z.Yang, L. Tong, Y. Bando and D. Golberg, *Adv. Mater.,* 2013, ***25***, 1109.

6 L. Viry, A. Levi, M. Totaro, A. Mondini, V. Mattoli, B. Mazzolai and L. Beccai, *Adv. Mater.,* 2014, ***26***, 2659.

7 K.Deng and L. Li, *Adv. Mater.,* 2014, ***26***, 2619.

8 F. F. Amos, S. A. Morin, J. A. Streifer, R. J. Hamers, and S. Jin, *J. Am. Chem. Soc.* 2007, ***129***, 14296.

9 Y. Aleava and B. Pianataro, *J. Mater. Chem. C*, 2014, ***2***, 6436.

10 X Cai, M. Peng, X. Yu, Y. P. Fu and D. C. Zou, *J. Mater. Chem. C*, 2014, ***2***, 1184.

11 A. Manekkathodi, M-Y. Lu, C. W. Wang and L-J. Chen, *Adv. Mater.,* 2010, ***22***, 4059-4063.

12 T. Zhang, X. Wang, T. Li, Q. Guo and J. Kang, *J. Mater. Chem. C*, 2014, **2**, 286; J. P Cheng, Y. J. Zhang and R. Y. Guo, *J. Cryst. Growth,* 2008, ***310***, 57-61.

13 D. I. Sa, H. Y. Yang, T. W. Kim and W. Park, *Appl. Phys. Lett*., 2013, ***102***, 021105.

14 X. Liu, L. L. Gu, Q. P. Zhang, J. Y. Wu, Y. Z. Long and Z. Y. Fan, *Nat. Commun.,* DOI: 10.1038/ncomms5007.

15 N. Liu, Z. D. Lu, J. Zhao, M. T. MacDowell, H-K Lee, W. Zhao, Y. Cui, *Nat. Nanotech.,* 2014, ***9***, 187.

16 H. L. Li, S. J. Jiao, H. T. Li and L. Li, *J. Mater. Sci.-Mater. Electron.,* 2014, ***25***, 2569.

17 X. Y. Zhang, J. Q. Qin, Y. N. Xue, P. F. Yu, B. Zhang, L. M. Wang and R. P. Liu, *Sci. Rep.* 2014, ***4***, 4596.

18 M. Ahmad, C. F. Pan, L. Gan, Z. Nawaz, and J. Zhu, *J. Phys. Chem. C,* 2010, ***114***, 243.

19 D. Gedamu, I. Paulowicz, S. Kaps, O. Lupan, S. Wille, G. Haidarschin, Y. K. Mishra and R. Adelung, *Adv. Mater.,* 2013, ***26***, 1541.

20 B. H. Kim and J. W. Kwon, *Sci. Rep.* 2014, ***4***, 4379.

21 C. Q. Zhu, B. G. Lu, Q. Su, E. Xie and W. Lan, *Nanoscale,* 2012, ***4***, 3060.

22 Y. Z. Zhang, Y. P. Liu, L. H. Wu, H. Li, L. Z. Han, B. C. Wang and E. Xie, *Appl. Surf. Sci.*, 2009, ***255***, 4801.

23 P. M. Ajayan, *Chem. Rev.,* 1999, ***99***, 1787.

24 Agarwal, *Planta,* 2006, ***224***, 1141.

25 O. Lupan, L. Chow, L. K. Ono, B. R. Cuenya, G. Y. Chai, H. Khallaf, S. Park, A. Schulte, *J. Phys. Chem. C,* 2010, ***114***, 12401.

26 X. D. Xue, T. Wang, X. D. Jiang, J. Jiang, C. X. Pan and Y. C. Wu, *CrystEngComm,* 2014, ***16***, 1207.

27 M. Guo, P. Diao and S. M. Cai, *Appl. Surf. Sci.,* 2005*,* ***249,*** 71.

28 G. Konstantators and E. H. Sargent, *Nat. Nanotechnol.* 2010, ***5***, 391.

29 K. W. Liu, J. G. Ma, J. Y. Zhang, Y. M. Lu, D. Y. Jiang, B. H. Li, D. X. Zhao, Z. Z. Zhang, B. Yao and D. Z. Shen, *Solid-State Electron.,* 2007, ***51***, 757.

30 Z. W. Jin, L. Gao, Q. Zhou and J. Z. Wang, *Sci. Rep.,* 2014, ***4***, 4268.

31 R. Yatskiv, J. Grym, K. Zdansky, K. Piksova, *Carbon*, 2012, ***10***, 3928; H. Zhang, A. V. Babichev, G. Jacopin, P.Lavenus, F. H. Julien, A. Y. Egorov, J.Zhang, T. Pauporté and M. Tchernycheva, *J. Appl. Phys*., 2013, ***114***, 234505; A. G. Ardakuni, M. Pazoki, S. M. Mahdavi, A. R. Bahnampour and N. Taghavinia, *App. Surf. Sci.,* 2012, ***258***, 5405.

32 Y. Takahashi, M. Kanamori, A. Kondoh, H. Minoura, Y. Ohya, *Jpn. J. Appl. Phys.,* 1994, ***33***, 6611.

33 J. Zhou, Y. D. Gu, Y. F. Hu, W. J. Mai, P-H. Yeh, G. Bao, A. K. Sood, D-L. Polla and Z. L. Wang, *Appl. Phys. Lett.* 2009, ***94***, 191103.

34 Y. Zheng, Z-Z. He, J. Yang, J. Liu, *Sci. Rep.* 2014, ***4***, 4588.

Graphical abstract for

Manuscript TC-ART-12-2014-002787 of

Journal of Materials Chemistry

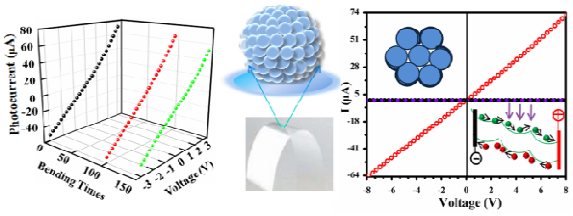

Grain and grain-boundary induced energy-edge modulated ZnO pomegranates-on-paper photodetector with large flexibility, low dark current, high responsivity and quick response.